# JOURNAL OF SOLID STATE CHEMISTRY

**Volume 179, Number 3, March 2006**


## CONTENTS

### *Regular Articles*



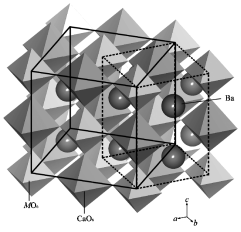


Crystal structures of $Ba_2CaMO_6$. Solid and dotted lines show the cubic cell and the tetragonal cell, respectively.



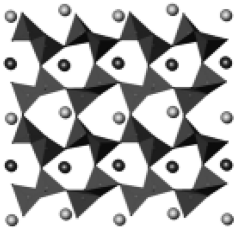

Structural studies of stuffed tridymite $AB_2O_4$ ($A$ = Ca, Sr and Ba and $B$ = Al and Ga) compounds indicate underbonding of the $A^{2+}$ sites. Attempts to dope the oxides with lanthanides invariably resulted in some segregation. These impurity phases are identified and their formation explained by bond valencies.



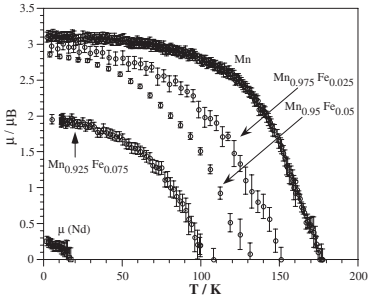


The Fe doping level greatly influences the double-exchange interaction on the ferromagnetic $Nd_{0.7}Pb_{0.3}Mn_{1-x}Fe_xO_3$ ($x$ = 0, 0.025, 0.05, 0.075, 0.1) phases. The structural and magnetic study has been carried out by neutron powder diffraction and susceptibility measurements performed between 1.7 and 300 K.

### *Regular Articles—Continued*



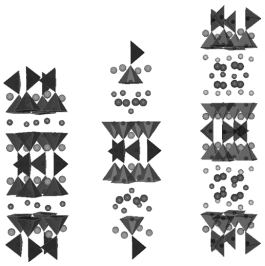

Crystal structures of the first three members of the Co-12$s$2 homologous series of multi-layered copper oxides; with increasing $s$ the number of (fluorite-structured) cation layers between the $CuO_2$ planes increases.



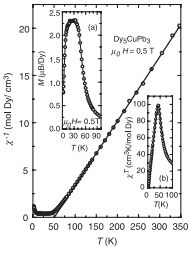


The magnetic susceptibility data for $Dy_5CuPb_3$.



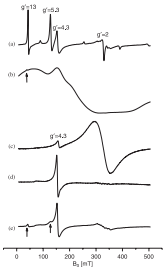

ESR spectra monitoring the process of corundum formation from boehmite xerogels via transition aluminas.

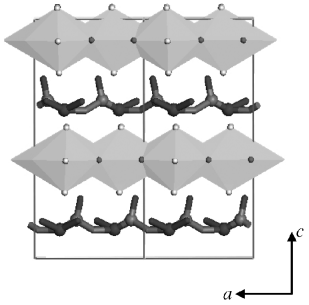


A polyhedral view showing the 1D chains of edge-sharing $[Zr(OH)_2F_3]^-$ pentagonal bipyramids. The anionic chains are charge-balanced by monoprotonated ethylenediamine cations, the latter displayed in ball-and-stick form.



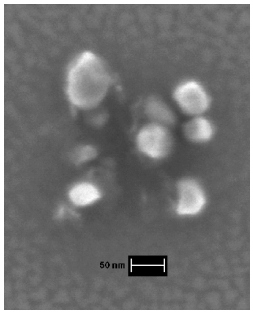


HR-SEM micrograph of $BaMoO_4$ nanopowders heat treated at 700 °C for 2 h.



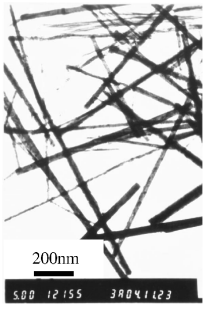


Single-crystalline nanorods of $\beta$-$MnO_2$, $\alpha$-$Mn_2O_3$ and $Mn_3O_4$ were successfully synthesized in large scale via the heat-treatment of $\gamma$-MnOOH nanorod precursors, which were prepared through a hydrothermal method in advance. Further experiments show that the as-prepared manganese oxide nanorods have catalytic effect on the oxidation and decomposition of the methylene blue (MB) dye with $H_2O_2$.



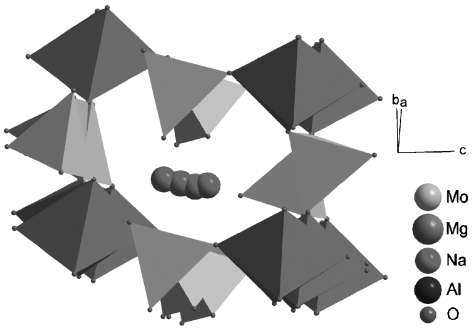


Crystal structure of $NaMg_3Al(MoO_4)_5$. The splitting of sodium position into four contributors in the cavity formed by Mo tetrahedra and Mg octahedra is shown.



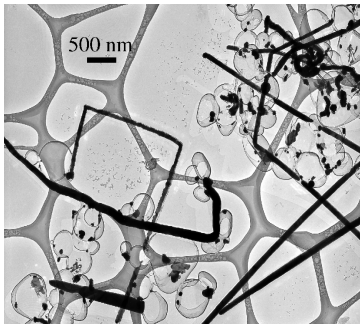


Long (100 μm or more) silver nanowires have been obtained at room temperature within 10–15 min using a procedure closely related to photographic film development.



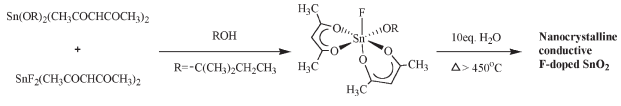


Synthetic route used to prepare nano-crystalline F-doped $SnO_2$.

*Continued*

**Synthesis and characterization of layered double hydroxides with a high aspect ratio**

Qi Tao, Yuanming Zhang, Xiang Zhang, Peng Yuan and Hongping He

***Page 708***

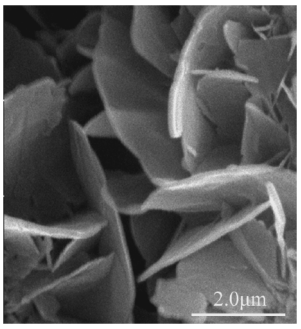


Layered double hydroxides with high aspect ratio were synthesized via a modified calcination-rehydration route. Rehydration of mixed oxides under suitable hydrothermal conditions shows effectiveness for preparation of stable thin sheet (ca. 35–60 nm) LDHs with a large size (ca. 0.5–6 μm).

---

**The transformation of ferrihydrite into goethite or hematite, revisited**

Yannick Cudennec and André Lecerf

***Page 716***

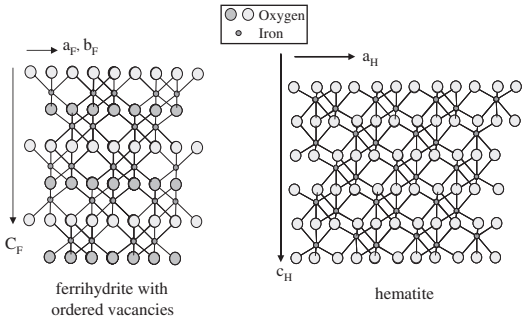


Relationship between ferrihydrite and hematite.

---

**A novel layered bimetallic phosphite intercalating with organic amines: Synthesis and characterization of $Co(H_2O)_4Zn_4(HPO_3)_6 \cdot C_2N_2H_{10}$**

Zhi-En Lin, Wei Fan, Feifei Gao, Naotaka Chino, Toshiyuki Yokoi and Tatsuya Okubo

***Page 723***

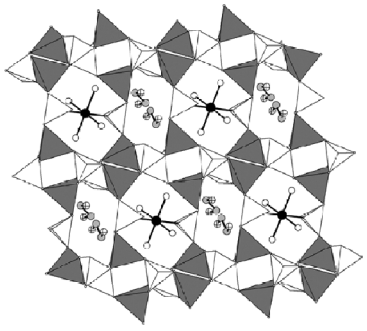

A new layered cobalt–zinc phosphite has been synthesized in the presence of ethylenediamine molecules as the structure-directing agents, which reside between the inorganic layers and can be exchanged by $NH_4^+$ cations.

**A novel high-temperature commensurate superstructure in a natural bariopyrochlore: A structural study by means of a multiphase crystal structure refinement**

L. Bindi, V. Petříček, R.L. Withers, M. Zoppi and P. Bonazzi

***Page 729***

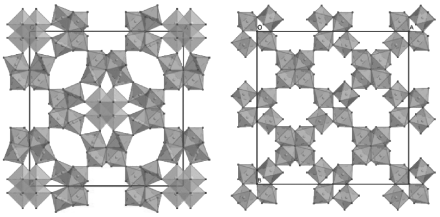

We report a new structure type related to that of pyrochlore containing three distinct types of corner-connected clusters, each made up of four individual $BO_6$ octahedra—the original tetrahedra of octahedra characteristic of the ideal pyrochlore-structure type, an 'opened out' version of this cluster and clusters of four $TiO_6$ octahedra forming small units of the NaCl structure type.

---

**Sol–gel-fluorination synthesis of amorphous magnesium fluoride**

J. Krishna Murthy, Udo Groß, Stephan Rüdiger, Erhard Kemnitz and John M. Winfield

***Page 739***

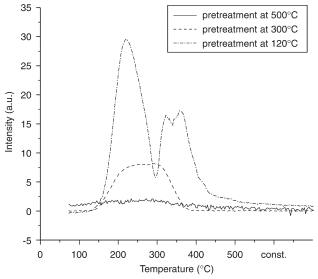


An amorphous high surface area magnesium fluoride (HS-$MgF_2$) can be prepared via a non-aqueous sol–gel route. It differs from crystalline $MgF_2$ remarkably in, e.g., exhibiting a substantial Lewis acidity as proved by $NH_3$-TPD. Because of its low crystallisation temperature, moderate preheating reduced the Lewis acidity drastically.

---

**A novel copper diphosphonate complex $Cu_4(aedp)_2(4,4'\text{-bpy})(H_2O)_4$ with three-dimensional framework structure**

De-Gang Ding, Ming-Cai Yin, Hui-Jie Lu, Yao-Ting Fan, Hong-Wei Hou and Yu-Ting Wang

***Page 747***

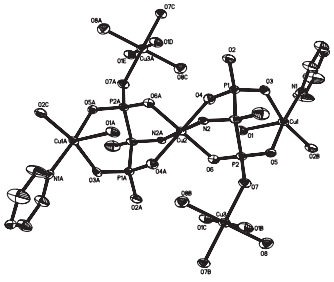

A novel copper diphosphonate complex $Cu_4(aedp)_2(4,4'\text{-bpy})(H_2O)_4$ has been hydrothermally synthesized and characterized, which adopts a three-dimensional framework structure assembled from $\{Cu_4(aedp)_2(H_2O)_4\}$ layers and 4,4′-bpy bridges. It shows typical antiferromagnetic behaviors at low temperature.

**The structure and ordering of ε-$MnO_2$**
Chang-Hoon Kim, Zentaro Akase, Lichun Zhang, Arthur H. Heuer, Aron E. Newman and Paula J. Hughes
***Page 753***

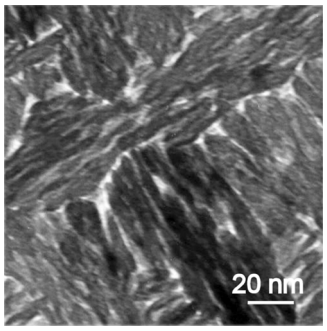


Bright-field TEM micrograph of a plan view foil from a 100% ε-$MnO_2$ sample after a 1 h/200 °C ordering heat treatment.

---

**Composition dependence of the structural chemistry and magnetism of $Ca_{2.5}Sr_{0.5}(Ga,Co)_{1+x}Mn_{2-x}O_8$**
Mathieu Allix, Peter D. Battle, Philip P.C. Frampton, Matthew J. Rosseinsky and Rocío Ruiz-Bustos
***Page 775***

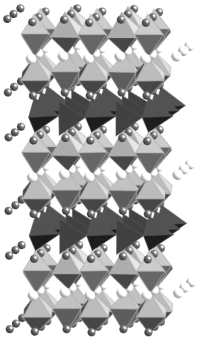

Crystal structure of $Ca_{2.5}Sr_{0.5}GaCo_{0.15}Mn_{1.85}O_8$. Polyhedral representation with octahedra and tetrahedra shaded light and dark, respectively. Light circles represent Ca/Sr cations, dark circles Ca only.

---

**Preparation and crystal structure of a new bismuth chromate: $Bi_8(CrO_4)O_{11}$**
N. Kumada, T. Takei, N. Kinomura and G. Wallez
***Page 793***

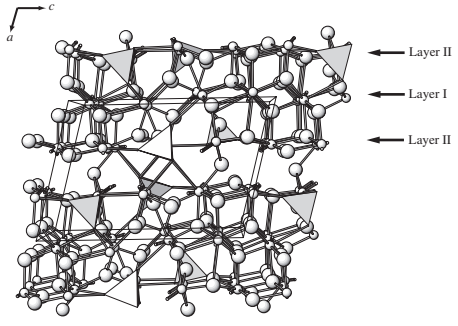


Crystal structure of $Bi_8(CrO_4)O_{11}$.

**Shape evolution of $SrCO_3$ particles in the presence of poly-(styrene-alt-maleic acid)**
Jiaguo Yu, Hua Guo and Bei Cheng
***Page 800***

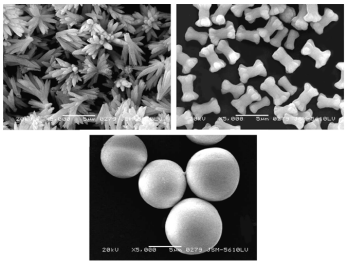

$SrCO_3$ particles with different morphologies, such as bundles, dumbbells, irregular aggregates and spheres were prepared by a simple precipitation reaction of sodium carbonate with strontium nitrate in the absence and presence of poly-(styrene-alt-maleic acid) (PSMA).

---

**Synthesis, characterization, and photocatalytic properties of $InVO_4$ nanoparticles**
Liwu Zhang, Hongbo Fu, Chuan Zhang and Yongfa Zhu
***Page 804***

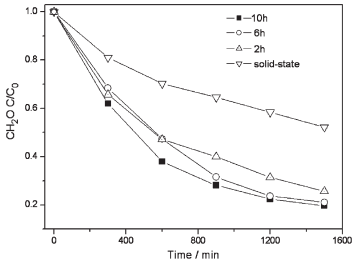


The catalytic activity for photodecomposition of FAD under visible light irradiation over $InVO_4$ obtained by calcining the complex precursor at 600 °C for various times and solid-state reaction at 1100 °C.

---

**Mixed oxides obtained from Co and Mn containing layered double hydroxides: Preparation, characterization, and catalytic properties**
František Kovanda, Tomáš Rojka, Jana Dobešová, Vladimír Machovič, Petr Bezdička, Lucie Obalová, Květa Jirátová and Tomáš Grygar
***Page 812***

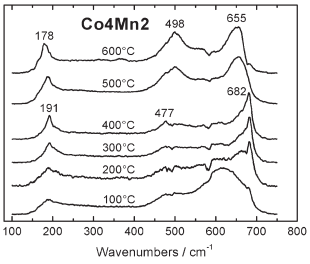


Raman spectroscopy revealed a segregation of Co-rich spinel in Co–Mn samples calcined at low temperatures.

*Continued*

**$Ga_3(HPO_3)_4F_4(H_3DETA)$ (DETA = diethylenetriamine): A new open-framework fluorinated gallium phosphite with pentameric building unit**

Li Wang, Tianyou Song, Yong Fan, Ying Wang, Jianing Xu, Suhua Shi and Tao Zhu

***Page 824***

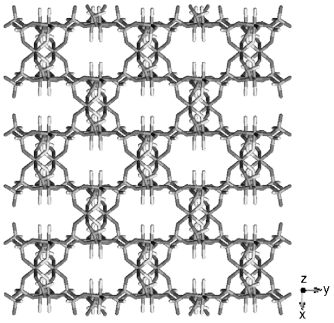


Perspective view of the structure of the title compound show 8-, 6- and 10-membered ring channels along [001].

---

**Synthesis, structure, and properties of four ternary compounds: CaSr*Tt*, *Tt* = Si, Ge, Sn, Pb**

Shengfeng Liu and John D. Corbett

***Page 830***

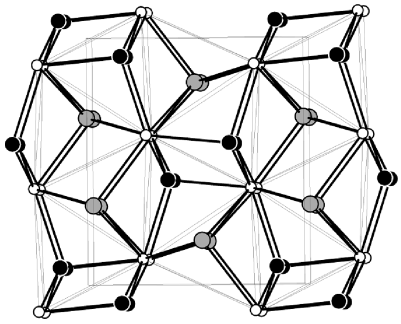

Mixed alkaline-earth-metal cations in this *inverse*-$PbCl_2$-type structure exhibit a clear differentiation as to their location and bonding in all of the tetrel phases Si–Pb.

---

**Crystal structure and magnetic properties of $Co_2TeO_3Cl_2$ and $Co_2TeO_3Br_2$**

Richard Becker, Helmuth Berger, Mats Johnsson, Mladen Prester, Zeljko Marohnic, Marko Miljak and Mirta Herak

***Page 836***

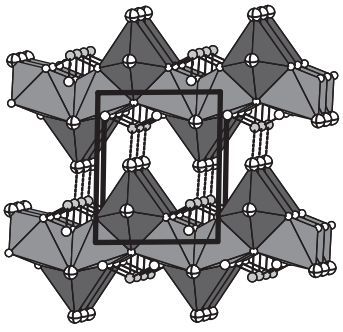

The Crystal structures and magnetic properties of two new layered compounds $Co_2TeO_3Cl_2$ and $Co_2TeO_3Br_2$ are presented. Both compounds show only weak van der Waal's forces connecting the layers and they both exhibit antiferromagnetic ordering below 30 K. The halogens and the lone-pairs on Te(IV) protrude from the layers.

**A low-temperature synthesis of ultraviolet-light-emitting ZnO nanotubes and tubular whiskers**

Jinping Liu and Xintang Huang

***Page 843***

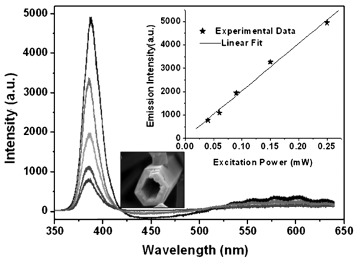


We have successfully synthesized single-crystal ZnO nanotubes and tubular whiskers by employing $Zn(NO_3)_2 \cdot 6H_2O$, $NH_3 \cdot H_2O$ as the starting materials in the presence of polyethylene glycol (PEG, $M_w = 2000$) at ambient pressure and low temperature (70 °C). These tubular products demonstrate a sharp ultraviolet excitonic emission peak centered at 385 nm at room temperature.

---

**Mixed crystals in the system $Cu_2MnGe_xSn_{1-x}S_4$: Phase analytical investigations and inspection of tetrahedra volumes**

Thomas Bernert, Manfred Zabel and Arno Pfitzner

***Page 849***

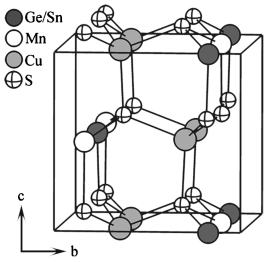


The system $Cu_2MnGeS_4$–$Cu_2MnSnS_4$ is inspected for the formation of mixed crystals at a temperature of 800 °C. The wurtzstannite structure type of $Cu_2MnGeS_4$ exists to 60% germanium content. The stannite structure type dominates from 20% germanium content to the pure Sn compound. Germanium and tin occupy a 2*a* position and are statistically disordered. Tetrahedra volumes [$MS_4$] of $Cu_2MnGe_{0.55}Sn_{0.45}S_4$ are compared with those of the end members and are used as a measure for the preference of the different structure type.

---

**MFI-type boroaluminosilicate: A comparative study between the direct synthesis and the templating method**

Wei Zhou, Shi-Yu Zhang, Xiang-Ying Hao, Hao Guo, Cui Zhang, Yin-Qing Zhang and Shuangxi Liu

***Page 855***

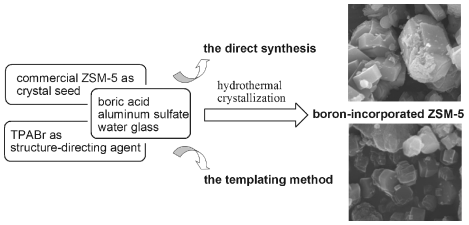


Boron-incorporated ZSM-5 zeolite was synthesized both via the direct synthesis and the templating method. The prepared B-ZSM-5 was characterized based on its structure, bonding, surface acidity, morphology, and chemical composition by a series of instrumental analysis and spectroscopic methods. The framework stability was investigated by the steam treatment. The differences in physicochemical properties of B-ZSM-5 prepared by the two methods were compared and discussed.

**Synthesis and characterization of three-dimensionally ordered macroporous ternary oxide**
S. Madhavi, C. Ferraris and Tim White
***Page 866***

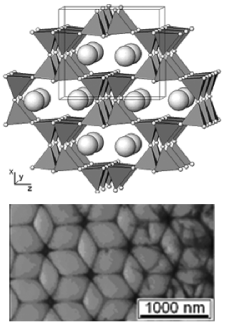


Framework structure of $CsAlTiO_4$ with Cs atoms located in the channels. Scanning transmission electron microscope (STEM) image of three-dimensionally ordered macroporous $CsAlTiO_4$.

---

**Formation and performances of porous $InVO_4$ films**
Shicheng Zhang, Chuan Zhang, Haipeng Yang and Yongfa Zhu
***Page 873***

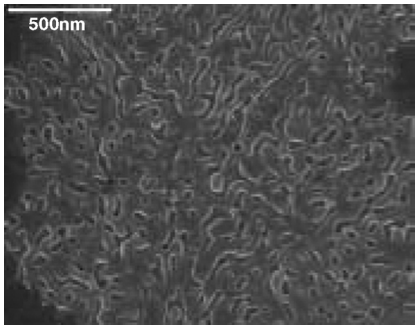


Porous $InVO_4$ film obtained from amorphous complex precursor under 500 °C.

---

**Two novel 3-D coordination polymers based on isonicotinic acid: Syntheses, crystal structures and fluorescence**
Bing Liu, Ling Xu and Guocong Guo
***Page 883***

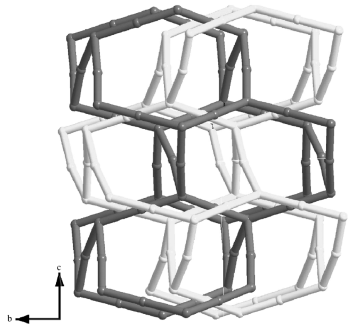

The hydrothermal reactions of HIso and metal salts yielded two novel 3-D coordination polymers $\{[Cu_4(Iso)_4(\mu_3\text{-}O)_2(C_2H_5OH)_2]\cdot 2C_2H_5OH\cdot C_2H_6N_4\}_n$ (**1**), $\{[Cd(Iso)_2(H_2O)]\cdot OHCCHO\}_n$ (**2**) (HIso = Isonicotinic acid), in which **1** was constructed from 32-membered rings and 3-D interpenetrating network of **2** from 42-membered rings.

**Synthesis and crystal structures of $Nd_6Pt_{13}In_{22}$, $Sm_6Pt_{12.30}In_{22.70}$, and $Gd_6Pt_{12.48}In_{22.52}$**
Vasyl I. Zaremba, Vitaliy P. Dubenskiy, Ute Ch. Rodewald, Birgit Heying and Rainer Pöttgen
***Page 891***

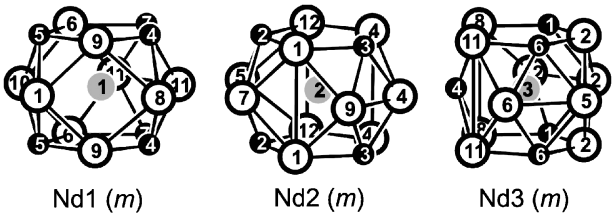


Coordination polyhedra of the neodymium atoms in $Nd_6Pt_{13}In_{22}$. Neodymium, platinum, and indium atoms are drawn as gray, black filled, and open circles, respectively. Nd1, Nd2, and Nd3 have site symmetry *m*.

---

**Phase segregation in the $Gd_{1-x}Sr_xFeO_{3-\delta}$ series**
Javier Blasco, Jolanta Stankiewicz and Joaquín García
***Page 898***

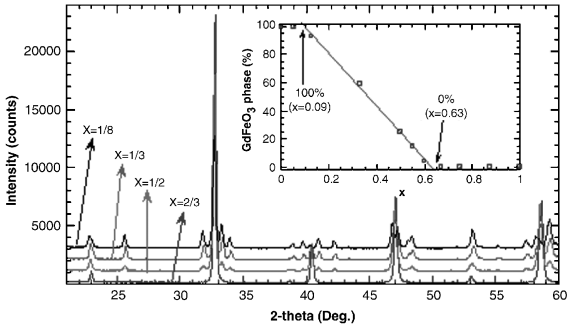


X-ray patterns for $Gd_{1-x}Sr_xFeO_{3-\delta}$ ($x = 1/8$, 1/3, 1/2 and 2/3). Inset: Content (in %) of the $GdFeO_3$-like phase in the $Gd_{1-x}Sr_xFeO_{3-\delta}$ samples. The straight line is a linear fit to the data for $3 \leqslant x \leqslant 0.6$ samples.

---

**Kinetic analysis of the thermal stability of lithium silicates ($Li_4SiO_4$ and $Li_2SiO_3$)**
Daniel Cruz, Silvia Bulbulian, Enrique Lima and Heriberto Pfeiffer
***Page 909***

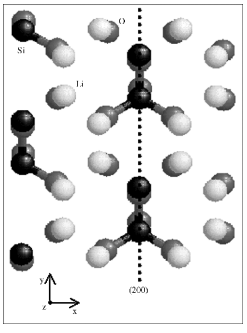


Scheme of the $Li_2SiO_3$ structure showing the [200] plane. From the darkest to the highlighted, the spheres represent silicon, oxygen and lithium atoms.

*Continued*

**Pressure-induced phase transition and octahedral tilt system change of $Ba_2BiSbO_6$**

Michael W. Lufaso, René B. Macquart, Yongjae Lee, Thomas Vogt and Hans-Conrad zur Loye

***Page 917***

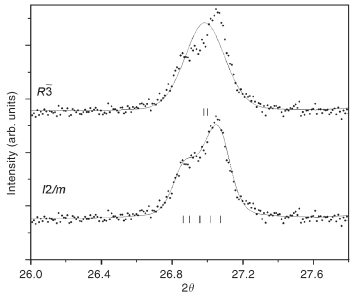


Fitting of the diffraction peaks of $Ba_2BiSbO_6$ is shown at an applied pressure of 6.1 GPa. The tick marks are the allowed positions of the Bragg reflections in space groups $R\bar{3}$ (top) and $I2/m$ (bottom), which illustrate the pressure-induced phase transition from space group $R\bar{3}$ at ambient pressure to the high-pressure $I2/m$ form.

---

**Spin-glass behavior in $Pr_{0.7}Ca_{0.3}CoO_3$ and $Nd_{0.7}Ca_{0.3}CoO_3$**

Asish K. Kundu, P. Nordblad and C.N.R. Rao

***Page 923***

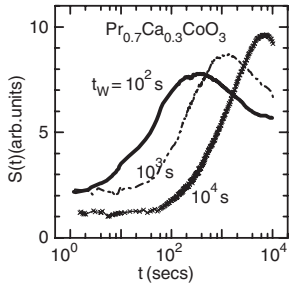


Spin-glass behavior of $Pr_{0.7}Ca_{0.3}CoO_3$ is indicated by the magnetic relaxation data.

---

**Room temperature synthesis and conductivity of the pyrochlore type $Dy_2(Ti_{1-y}Zr_y)_2O_7$ ($0 \leqslant y \leqslant 1$) solid solution**

Karla J. Moreno, Manuel A. Guevara-Liceaga, Antonio F. Fuentes, Javier García-Barriocanal, Carlos León and Jacobo Santamaría

***Page 928***

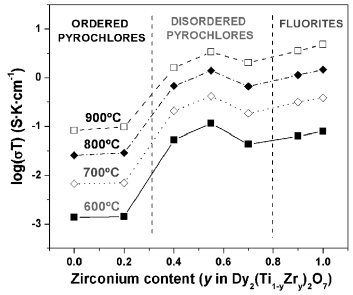


Conductivity dependence and structural evolution with Zr content for $Dy_2(Ti_{1-y}Zr_y)_2O_7$ ($0 \leqslant y \leqslant 1$). The increase in conductivity of more than one order of magnitude when $0 < y < 0.4$ is related to the onset of disordering of the oxygen sublattice of the ideal pyrochlore structure.

**Single-crystal growth of $Tl_2Ru_2O_7$ pyrochlore using high-pressure and flux method**

Daisuke Mori, Noriyuki Sonoyama, Atsuo Yamada, Ryoji Kanno, Masaki Azuma, Mikio Takano, Katsumi Suda and Nobuo Ishizawa

***Page 935***

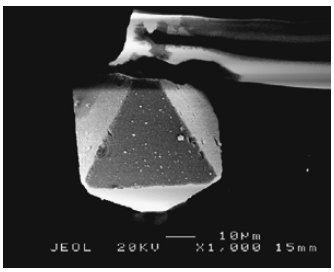


SEM photograph of a single crystal of $Tl_2Ru_2O_7$ pyrochlore.

---

**Synthesis and characterization of the pseudo-hexagonal hollandites $ALi_2Ru_6O_{12}$ ($A$ = Na, K)**

M.L. Foo, T. He, Q. Huang, H.W. Zandbergen, T. Siegrist, G. Lawes, A.P. Ramirez and R.J. Cava

***Page 941***

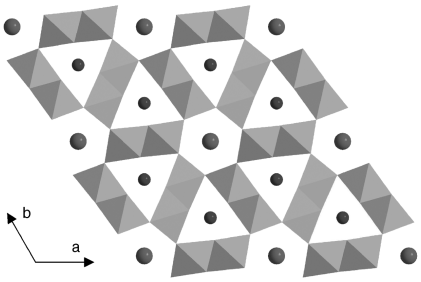


The crystal structure of $NaLi_2Ru_6O_{12}$ with emphasis on the $RuO_6$ octahedra (cyan). Na (magenta) and Li ions (blue) are located in hexagonal and triangular channels, respectively. This new hollandite structure type has pseudo-hexagonal symmetry.

## *Rapid Communications*

**The influence of intercalation rate and degree of substitution on the electrorheological activity of a novel ternary intercalated nanocomposite**

Bao-Xiang Wang and Xiao-Peng Zhao

***Page 949***

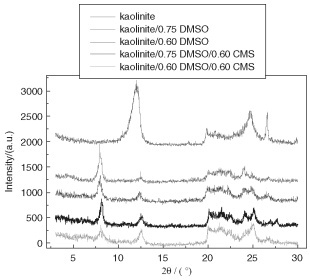


Kaolinite/dimethylsulfoxide (DMSO)/carboxymethyl starch (CMS) ternary nanocomposites were prepared according to the combination of intercalation and solution reaction. At the suitable component ratio of ternary nanocomposite the optimum electrorheological (ER) effect can be attained. It is apparent that the notable ER effect of ternary ER fluid was attributed to the prominent dielectric property of the ternary nanocomposite ERF, which is closely associated with the intercalation rate (IR).

**Synthesis and photoluminescence of single crystals europium ion-doped $BaF_2$ cubic nanorods**
Gejihu De, Weiping Qin, Jisen Zhang, Jishuang Zhang, Yan Wang, Chunyan Cao and Yang Cui
***Page 955***

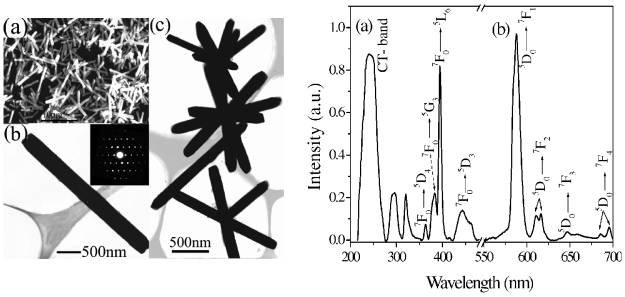


Fig. 2: (a) SEM image of the $BaF_3:Eu^{3+}$ nanorods. (b) TEM image of an individual $BaF_3:Eu^{3+}$ nanorod. Inset: Electron diffraction patterns of the nanorods. (c) TEM image of $BaF_3:Eu^{3+}$ nanopropellers. Fig. 3: (a) Excitation spectra of $BaF_2:Eu^{3+}$ nanorods, monitored at 614.5 nm emission position at room temperature. (b) Emission spectra of $BaF_2:Eu^{3+}$ nanorods under 393 nm excitation at room temperature.

## NOTICE

The Keyword Index for Volume 179 will appear in the December 2006 issue as part of a cumulative index for the year 2006.